Enhancing Ischemic Brain Stroke Detection on CT Images: A Investigation of Transfer Learning Techniques of DenseNet-201 for Neuroimaging Analysis

1st Chathura D. Kulathilake
Dept. of Radiological Sciences
School of Human Health Sciences
Tokyo Metropolitan University
Tokyo, Japan
cdchathu@gmail.com

2nd Jeevani Udupihille
Dept. of Radiology
Faculty of Medicine, University of Peradeniya
Peradeniya, Sri Lanka
jeevani.uduphille@med.pdn.ac.lk

3rd Atsushi Senoo
line 2: *Dept. of Radiological Sciences*
School of Human Health Sciences
Tokyo Metropolitan University
Tokyo, Japan
senoo@tmu.ac.jp

***Abstract*—Over the past few decades, strokes, also called cerebrovascular diseases or cerebral vascular accidents (CVAs), have become a significant contributor to morbidity and mortality globally. Brain stroke early diagnosis is vital to initiate treatment to prevent brain cells from becoming necrotic. Non-contrast-enhanced computed tomography (NCCT) is the primary imaging technique used to diagnose brain stroke conditions. Deep learning-based computer-aided diagnoses are developed to aid in diagnosis as 'the brain is time'. DenseNet201 architecture has alleviated the issue of gradient vanishing by utilizing dense connections. This study aims to detect brain stroke conditions by developing two deep learning models utilizing the transfer learning architecture of DenseNet201. Two deep learning models serve as a two-step process to identify ischemic stroke and its subtype conditions. Model 01 achieved an intrinsic accuracy of 97. 03% in the training set, 94. 50% in the validation set. Also, test and test time augmentation accuracy (TTA) was 94.50%. Model 02 reached an intrinsic accuracy of 98.02% in the training set and 95.67% in the validation set. Further, the test and TTA accuracy were 95.67%.**

Keywords—Brain stroke, Deep learning, Computed tomography, Transfer learning, Computer-aided diagnosis

I. Introduction

Stroke is one of the main causes of adult disability and the second leading cause of mortality worldwide [1,2]. A stroke, medically referred to as a cerebrovascular accident (CVA), happens when there is a sudden cessation of blood circulation to a specific area of the brain, resulting in the impairment or death of brain cells [3]. There are two primary categories of strokes: ischemic stroke and hemorrhagic stroke are two types of strokes [4]. An ischemic stroke occurs due to an obstruction or clot in a blood artery that provides blood to the brain [5]. The obstruction can arise from the formation of a blood clot (thrombus) within a cerebral blood artery or the migration of a clot (embolus) from another part of the body to the brain [6]. A hemorrhagic stroke happens when there is the presence of blood leakage within or in the vicinity of the brain [7]. The occurrence of bleeding can be attributed to either a hemorrhage, which is the rupture of a blood vessel, or the bursting of an aneurysm, which is a weakened, balloon-like section in the wall of a blood artery [8].

Stroke imaging is crucial for detecting the patient's condition, ruling out hemorrhagic stroke and other disorders that mimic similar conditions, such as benign tumors and infections, and initiating thrombolysis therapy [9]. Early detection of a cerebral stroke is imperative to preserve the patient's life and mitigate any undesirable consequences. Magnetic resonance imaging (MRI) and computed tomography (CT) are commonly employed medical imaging techniques for diagnosing strokes [10]. These instruments use distinctive methods to image different anatomical structures and abnormalities accurately. [11]. Due to its higher availability compared to MRI scanners, CT scanners are primary and essential medical imaging devices [12]. In addition, there are other medical advantages, such as faster image acquisition, improved usability for patients with severe injuries, and heightened ability to detect or confirm hemorrhagic stroke [13,14]. Additionally, it has the capability to do multimodal CT examinations, including non-enhanced CT, perfusion CT, and CT angiography [15].

Computer-aided diagnosis (CAD) plays a vital role in medical image analysis, enabling radiologists to evaluate and interpret abnormalities and facilitating timely therapy initiation [16]. Classical machine learning methods have been employed in computer-aided diagnosis (CAD) for many years to detect, categorize, and differentiate different medical states. Furthermore, some computer-assisted techniques and tools have been developed during the past decade to identify brain abnormalities at the earliest possible stage. Deep Learning is commonly used to recognize strokes accurately and automatically [17]. This study is focused on detecting and classifying brain stroke conditions considering the type of brain stroke depending on the radiological features and on set time, as shown in the Table I. Significantly, the effectiveness of each of the stroke therapies diminishes over time until the potential for consequences surpasses their advantages. Therefore, the current recommendations impose restrictions on the timing of administering some medications. Thrombolysis can be administered within 4.5 hours from the beginning of symptoms [18]. Hence, a precise understanding of time is crucial for stroke treatment. Therefore, two deep learning models were developed in which the model 01 is to classify brain ischemic, hemorrhagic, and normal conditions, and the model 02 is to classify acute, subacute, and chronic conditions depending on the on-set time shown in Fig. 1.

979-8-3503-5409-6/24/$31.00 ©2024 IEEE
DOI 10.1109/CAI59869.2024.00101

Further, this study investigated DenseNet-201 transfer learning architecture performances concerning radiological feature detection on brain CT stroke images. In the DenseNet-201 architecture, deep layers are anticipated to apprehend more sophisticated and advanced characteristics crucial for comprehending the elaborate patterns found in medical images. Therefore, feature maps from deeper layers can capture intricate features and subtle patterns that can indicate brain strokes.

The DenseNet was developed to overcome some constraints of conventional designs such as VGG and ResNet. Researchers are concerned about the issue of gradient vanishing as the number of layers of the network in CNN models continues to increase. Batch normalization partially mitigates the issue of gradient vanishing [19]. DenseNet establishes dense connections by directly linking each layer to every other layer in a feed-forward manner. This architectural design promotes the reuse of features, decreases the quantity of parameters, and improves the flow of gradients throughout the training process. DenseNet introduced the concept of dense connectivity, composed of dense blocks, bottleneck layers, transition blocks, and global average pooling [20].

Fig. 1. Brain CT axial image: (a). Normal condition, (b). Ischemic condition,

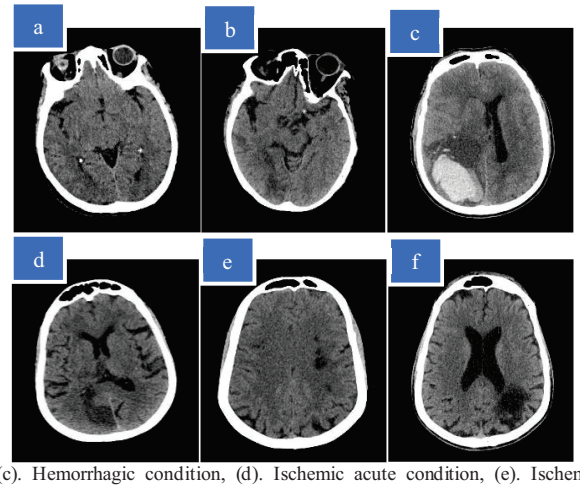

(c). Hemorrhagic condition, (d). Ischemic acute condition, (e). Ischemic subacute condition, (f). Ischemic chronic condition (Source: Kandy National Hospital, GE Medical System- Revolution EVO)

TABLE I. RADIOLOGICAL FEATURES ON NCCT IMAGES BASED ON STROKE TYPE AND ON-SET TIME

Stroke type (on-set time)	Radiological features
Ischemic - acute (0-7 days)	Loss of gray-white matter differentiation, hypo attenuation of deep nuclei [23]
Ischemic - subacute (1-3 Weeks)	Attenuation of the cortex, clearly demarcated infarcted area, edema mass effect (maybe) [23]
Ischemic - chronic (> Weeks)	Hypodense areas, ventricular enlargement, atrophy and encephalomalacia (affected areas) [23]
Hemorrhagic - acute (0-7 days)	Hyperdense with fluid levels, mass effect and mid-line shift [24]
Hemorrhagic - subacute (1-3 Weeks)	Less intense with a ring-like appearance, surrounding edema and mass effect [24]
Hemorrhagic - chronic (> 3 Weeks)	Iso dense or confined hypo density, atrophy and encephalomalacia (maybe developed) [24]

Lisowka et al. conducted an ischemic stroke detection investigation using 170 CT datasets in 2017. The CNN technique was employed in this work, and the hinge loss function was used in the algorithm development phase. This study also used the ADAM optimizer and Keras with the Theano framework. The crucial validation step was carried out by dividing the data set into 71 participants for training, 51 individuals for testing, and 48 subjects for validation. The accuracy of the study was 96.4% [21].

Lo et al. have proposed a classification model that uses 1254 grayscale CT scans from 96 patients with acute ischemic stroke (573 images) and 121 healthy controls (681 images) of NCCT. The transfer learning method is adopted to overcome the limited data size. AlexNet without pre-trained parameters achieved an accuracy of 97.12%, a sensitivity of 98.11%, a specificity of 96.08%, and an area under the receiver operating characteristic curve (AUC) of 0.9927. [22].

II. MATERIALS AND METHODS

The ethical approval was obtained from the Ethics Review Committee, Faculty of Allied Health Sciences, University of Peradeniya, and Tokyo Metropolitan University, Japan, to gather data and carry out the study. The data set was gathered retrospectively from two Sri Lankan hospitals during 2017 and 2022, which Anuradhapura Teaching Hospital has Aquilion, Toshiba CT scanner, and Kandy National Hospital has Revolution EVO, GE Medical System. The CT scan images containing artefacts were eliminated based on the inclusion and exclusion criteria. The study included individuals aged 20 to 80 years whose CT scan data were utilized. Patients with conditions other than brain stroke were also eliminated based on their medical history. The control class of normal brain condition contained CT DICOM images ranging from just above the foramen magnum to the vertex of the brain. The data set contained 2819 ischemic stroke conditions, 2548 hemorrhagic stroke conditions and 2819 normal conditions of NCCT (non-contrast-enhanced computed tomography) images.

A. Data Pre-processing

The obtained CT brain data were anonymized using the Python program as CT DICOM images contained pixels and metadata (patient data). CT axial brain data sets were pre-processed, applying labelling as a supervised learning task, intensity normalization, and resampling as data was collected from the two different CT scanners in two hospitals and windowing. In addition, data augmentation was implemented during the model training process. The dataset was divided into training (3567 images, 74.82%), test sets (600 images, 12.58%), and validation (600 images, 12.58%) for model 01. Further, the ischemic data set was divided into training (1619 images, 57.43%), test sets (600 images, 21.28%) and validation (600 images, 21.28%) for model 02. The CT images of 512×512 matrix sizes were resized to 460×460 pixels to match the input size of the pre-trained DenseNet model.

B. *DenseNet Architecture, Design and Training*

The environments in which the two deep learning models were developed and implemented are detailed in Table II. Two deep learning models were developed, including the 4767 CT brain images. The two models work as two-step deep learning models to classify brain normal, ischemic, and hemorrhagic conditions by model 01, while acute, subacute, and chronic conditions of ischemic condition by model 02. The architecture comprises convolutional layers, max pool, dense layers (completely connected layers), and transition layers. The model's architecture is executed using the ReLU activation function, with SoftMax activation being employed for the concluding layer. A 1-cycle policy and FastAI were implemented to facilitate faster convergence to the solution and attain a higher training rate.

Further, test-time augmentation was applied, which involved generating several augmented iterations of every test image and feeding each enhanced iteration into the model to obtain a prediction. The ultimate forecast for each test image is often the meaning of the estimates derived from all the enhanced iterations of that image. The final layer of DenseNet was modified to get the required output for both models. Each model's final layer was changed to obtain the desired output, which consists of three classes. The FastAI's Lerner class were set up for the training process, which finds the suitable learning rate (Fig. 2) and then trains the model using a 1-cycle policy. The following hyperparameters were defined for each model, as mentioned in Table II. The following accuracies were measured in each model: intrinsic training, validation accuracy, test accuracy, test time augmentation accuracy (TTA). The model's performance was evaluated using recall, precision, accuracy, and F1 score metrics. The Grad-CAM (Gradient-weighted Class Activation Mapping) technique was applied to the two models to visualize the region of the input image that contribute most significantly to the model's predictions.

TABLE II. SPECIFICATIONS OF THE MODEL IMPLEMENTED ENVIRONMENT

Environment	Specifications
Operating system	Microsoft Windows 11 Home (22H2)
Processor	Intel(R) Core (TM) i7-9750
Architecture	64-bit
Memory	32 GB
GPU	NVIDIA GeForce GTX 1650
Language	Python
Framework	PyTorch, DL
Libraries used.	Pydicom, cv2, os, Matplotlib, Pandas, Scikit-learn

TABLE III. HYPERPARAMETER VALUES ASSOCIATED WITH TWO DENSENET-201 MODELS

Hyperparameter	Tuned value
Batch size	32
Initial learning rate	0.001
Activation	ReLU, SoftMax
Optimizer	Adam
Loss function	Cross Entropy

III. RESULTS

In this study, we analyzed brain stroke detection using DenesNet201 architecture. The two deep learning models were utilized as a two-step process. The model 01 intrinsic training accuracy and validation accuracy were 97.03% and 94. 50% respectively. The intrinsic test accuracy and TTA test accuracy for model 01 were 94.50% and 94.50%, respectively. In contrast, model 02 test intrinsic training accuracy and validation accuracy were 98.02% and 95.67%, respectively. The intrinsic and TTA test accuracy for model 01 was 95.67%.

The learning rates were obtained by learning rate finder curves (LR finder) as the steepest descent points were 0.0275 and 0.0831 for models 01 and 02, respectively (Fig 2). The total trainable parameters were 5,763 for both models out of 18,098,691 parameters.

Training and validation loss per epoch and training and validation accuracy per epoch curves were plotted by both models in Fig. 4 and Fig. 5 to analyze the underfitting or overfitting conditions of the models, and there were no such conditions on either model. Therefore models 01 and 02 both training and validation loss curves showed consistent pattern which suggests that the model is generalizing well to unseen data. The model 01 and 02 confusion matrices are shown in Fig. 3. The performances of our two models were evaluated mainly using confusion matrix and accuracy. In addition to that precision, recall and false positive rate (FPR) were calculated which is shown in Table IV for both models.

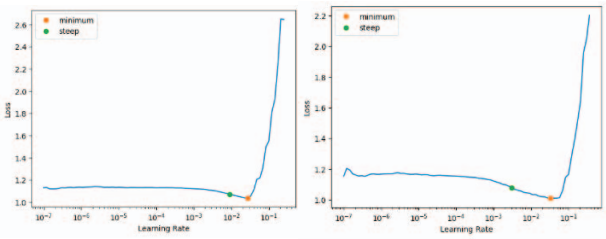

(a) (b)

Fig. 2. Learning rate curve vs loss curve (a). Model 01 curve, (b). Model 02 curve.

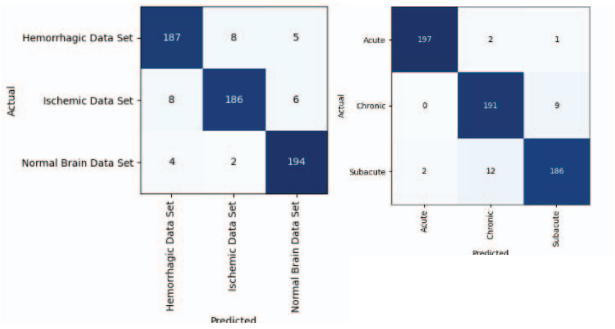

Model 01 Model 02

Fig. 3. Confusion matrix of model 01 and model 02.

The confusion matrix was obtained to analyze the performances of the two models' class-wise. Table IV shows that model 01 has high accuracy, F1-score, precision, specificity, and recall for all three classes, indicating a robust overall performance. The confusion matrix was obtained to analyze the performances of the two models' class-wise. Table IV shows that model 01 has high accuracy, F1-score, precision, specificity, and recall for all three classes, indicating a robust overall performance.

TABLE IV. MODEL'S PERFORMANCES MATRICES

Parameter	Model 01				Model 02			
	H[a]	Ischemic	Normal	Average	I. Acute[b]	I. Subacute[c]	I. Chronic[d]	Average
Accuracy (%)	95.83	96	97.16	96.33	99.16	96	96.16	97.11
F1-Score (%)	93.5	93.93	95.8	94.41	98.74	93.93	94.32	95.66
Precision (%)	93.96	94.898	94.63	94.5	98.99	94.89	93.17	95.68
Specificity (%)	97	97.5	97.25	97.25	99.5	97.5	96.5	97.83
Recall (%)	93.5	93	97	94.5	98.5	93	95.5	95.66
False Positive Rate (FPR) (%)	3.09	2.5	2.75	2.78	0.5	2.5	3.5	2.16

[a]Hemorrhagic; [b]Ischemic acute; [c]Ischemic subacute; [d]Ischemic chronic

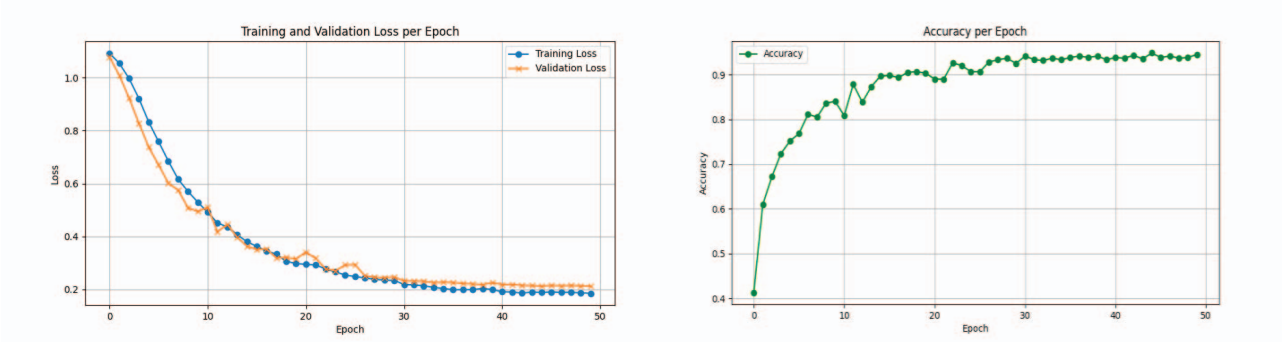

(a) (b)

Fig. 4. (a). Training and validation loss per epoch, (b). Training and validation accuracy per epoch curves for model 01.

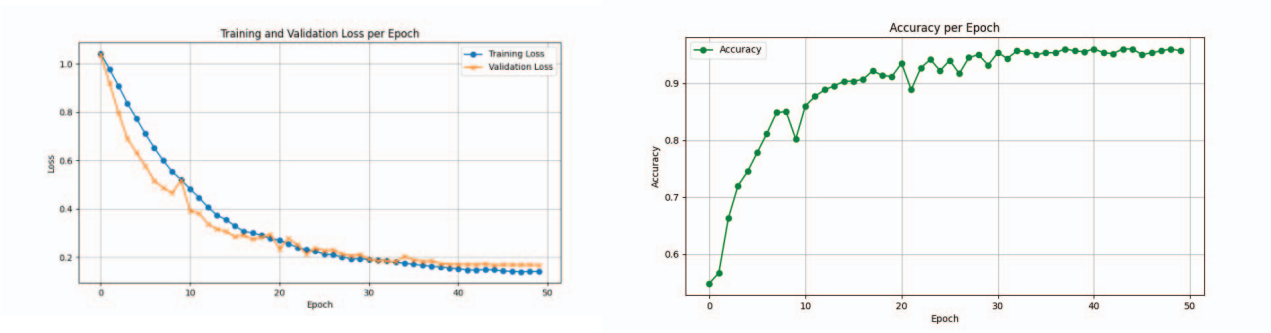

(a) (b)

Fig. 5. (a). Training and validation loss per epoch, (b). Training and validation accuracy per epoch curves for model 02.

Although the model exhibits strong performance across all classes, it demonstrates slightly lower precision, recall, and FPR performances for ischemic cases compared to hemorrhagic and normal brain conditions. In model 01, average precision and recall were 94.5%, indicating that false positive and false negative have the same impact. Model 01 average F1-score was 94.41%. Model 02 average accuracy, average precision, average specificity, and F1-score were 97.77%, 95.68%, 97.83%, and 95.66%, respectively, which generally outperforms model 01 regarding accuracy, precision, specificity, and F1-score.

FPRs were less than 4% for each class in the two models, which indicates that less than 4% of the actual negative instances were incorrectly predicted as positive. In model 02, ischemic acute class FPR is 0.5%.

The receiver operating characteristics (ROC) curves for model 01, as shown in Fig. 6, exhibited a value of 0.99 for hemorrhagic and ischemic classes and 1.00 for normal conditions, indicating that the model has a high true positive rate and a low false positive rate for distinguishing between positive and negative instances. The ROC curves of model 02 displayed values of 1.00, 0.99, and 0.99 for acute, subacute, and chronic classes, respectively, which indicate that the model demonstrates exceptional performance in differentiating instances corresponding to different classes, with notable sensitivity and specificity.

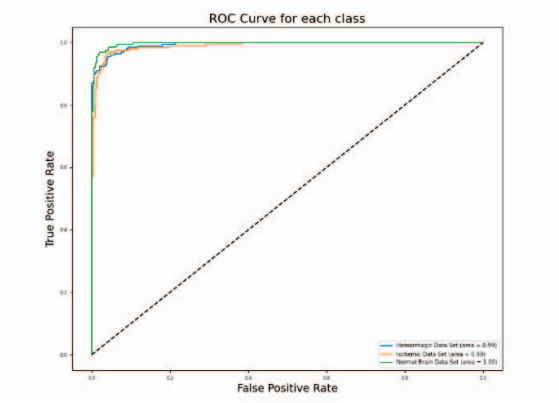

(a)

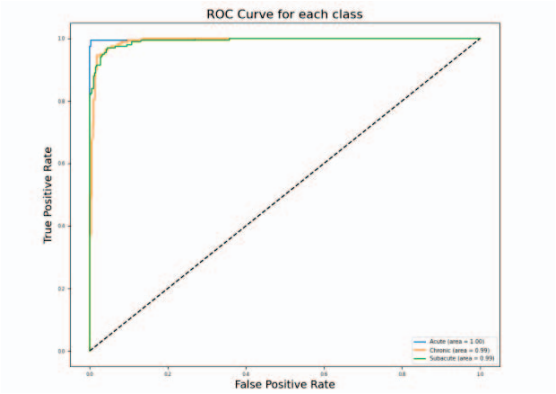

(b)

Fig. 6. The AUC curves, (a). Model 01, (b). Model 02.

Figures 7 and 8 show each model's top five losses were obtained to analyze the model prediction, actual outputs, and its error detection of radiological features. In model 01, four incidence errors predict brain hemorrhagic conditions as normal condition with high confidence among the top five (Table V). In these four cases, hyper-dense areas of the brain parenchyma due to blood were detected as normal radiological features of the brain. In model 02, adjacent subtypes were predicted as wrong predictions, especially subacute cases, which were predicted as chronic conditions (Table VI).

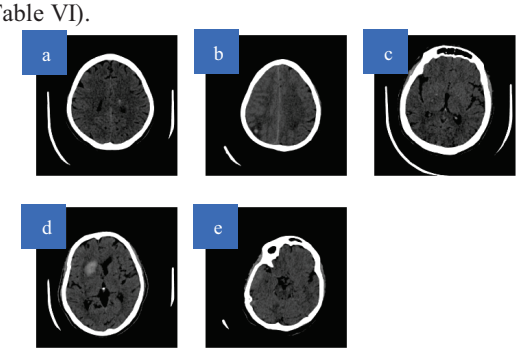

Fig. 7. Top five losses of model 01.

TABLE V. EVALUATION OF TOP FIVE LOSSES OF MODEL 01

Image	Prediction	Actual	Loss	Probability
(a)	Normal	Hemorrhagic	3.18	0.96
(b)	Normal	Hemorrhagic	3.09	0.95
(c)	Normal	Hemorrhagic	2.16	0.79
(d)	Normal	Hemorrhagic	2.15	0.86
(e)	Ischemic	Normal	2.01	0.66

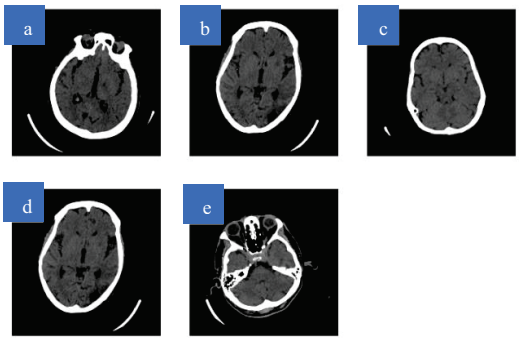

Fig. 8. Top five losses of model 02.

VI. EVALUATION OF TOP FIVE LOSSES OF MODEL 02

Image	Prediction	Actual	Loss	Probability
(a)	Chronic	Acute	3.12	0.90
(b)	Chronic	Subacute	3.07	0.94
(c)	Subacute	Chronic	1.81	0.71
(d)	Chronic	Subacute	1.62	0.79
(e)	Acute	Subacute	1.49	0.41

Figure 9 shows selected output images of Grad-CAM that applied for the final convolutional layer of model-01 (Denseblock4-Denselayer32-Conv-2).

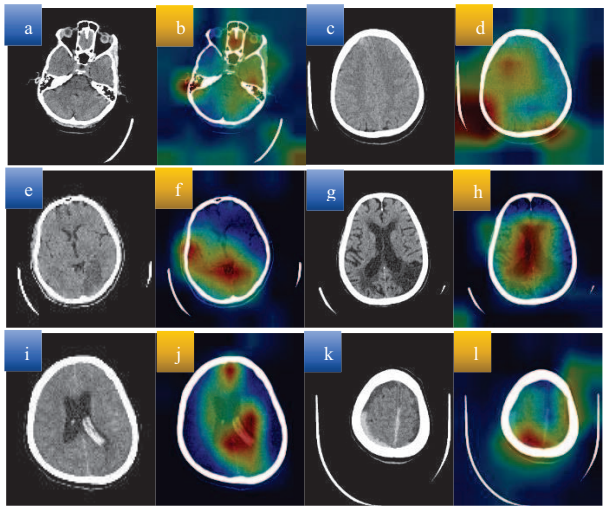

Fig. 9. The Grad-CAM Images extracted from the final convolutional layer (denseblock4-denselayer32-conv-2) of model -01: (a). & (c). Normal brain conditions, (b) & (d). Corresponding Grad-CAM output of a & c, (e). & (g). Ischemic stroke conditions, (f) & (h). Corresponding Grad-CAM output of e & g, (i). & (k). Ischemic conditions, (j) & (l). Corresponding Grad-CAM output of i & k.

IV. DISCUSSION

The overall NCCT data set comprised a total of 4767 images. Hence, a pre-trained transfer learning architecture was employed to address the class imbalance issue due to the limited number of reported ischemia acute cases. The DICOM file format was utilized as input and subsequently transformed into a compatible format for the DenseNet-201 architecture. The 1-cycle policy was included during the implementation phase of the architecture to enhance the learning process. It involves starting with a lower learning

rate, gradually increasing it for the first half, and then gradually decreasing it for the second half. The FastAI library integrates the 1-cycle policy, facilitating researchers' ability to experiment with and deploy cutting-edge deep learning models readily. There are some limitations related to this work. Stroke data were obtained from two CT scanners in two hospitals. Prior research has demonstrated substantial variation among scanners and manufacturers. As a result of its fundamental 2D nature from CT axial images, the performance of the proposed model may be constrained, as it is possible that certain aspects cannot be adequately captured due to its incapacity to utilize the entire 3D volume. Though artefacts containing data were omitted in the inclusion criterion phase, no investigation was conducted about the noise of the CT data. Inherent electronic noise of the CT images would significantly affect the feature extraction phase, though the different filters used to process the images and electronic noise would lead to misleading radiological features on CT images. The acquired Grad-CAM visualizations emphasize specific regions linked to brain stroke disorders, displaying prominent activation patterns in affected areas. In contrast, the Grad-CAM highlights are more moderate in normal conditions and distributed throughout the corresponding images.

V. CONCLUSIONS AND FUTURE WORKS

In this study, we have proposed the multi-class classification of brain stroke using NCCT images. Further, DenseNet201 architecture was selected as the neural network architecture according to the literature, different parameters were tested, and evaluation metrics were recorded. The 1-cycle policy and FastAI were adopted to the network to facilitate faster convergence to the solution and attained a higher training rate. The DenseNet201 architecture with the FastAI technique was more successful than traditional and task-specific algorithms. Future endeavors involve conducting brain stroke age detection by density changes of the brain parenchyma with more clinical validation studies and investigating the potential expansion of the model to three-dimensional (3D) applications.

ACKNOWLEDGEMENT

The authors thank hospital staff from Anuradhapura Teaching Hospital and Kandy National Hospital in Sri Lanka for their support in the data collection phase.

REFERENCES

[1] V. L. Feigin et al., "Global, regional, and national burden of neurological disorders, 1990–2016: a systematic analysis for the Global Burden of Disease Study 2016," The Lancet Neurology, vol. 18, no. 5, pp. 459–480, May 2019, doi: 10.1016/s1474-4422(18)30499-x.

[2] C. O. Johnson et al., "Global, regional, and national burden of stroke, 1990–2016: a systematic analysis for the Global Burden of Disease Study 2016," The Lancet Neurology, vol. 18, no. 5, pp. 439–458, May 2019, doi: 10.1016/s1474-4422(19)30034-1.

[3] M. E. Watts, R. Pocock, and C. Claudianos, "Brain Energy and Oxygen Metabolism: Emerging Role in Normal Function and Disease," Frontiers in Molecular Neuroscience, vol. 11, Jun. 2018, doi: 10.3389/fnmol.2018.00216.

[4] N. R. Wevers et al., "Modeling ischemic stroke in a triculture neurovascular unit on-a-chip," Fluids and Barriers of the CNS, vol. 18, no. 1, Dec. 2021, doi: 10.1186/s12987-021-00294-9.

[5] Z. Liu et al., "Engineering Neurovascular Unit and Blood–Brain Barrier for Ischemic Stroke Modeling," Advanced Healthcare Materials, vol. 12, no. 19, May 2023, doi: 10.1002/adhm.202202638.

[6] Y. Xiong, A. K. Wakhloo, and M. Fisher, "Advances in Acute Ischemic Stroke Therapy," Circulation Research, vol. 130, no. 8, pp. 1230–1251, Apr. 2022, doi: 10.1161/circresaha.121.319948.

[7] A. Montaño, D. F. Hanley, and J. C. Hemphill, "Hemorrhagic stroke," Interventional Neuroradiology, pp. 229–248, 2021, doi: 10.1016/b978-0-444-64034-5.00019-5.

[8] V. T. Lehman et al., "Conventional and high-resolution vessel wall MRI of intracranial aneurysms: current concepts and new horizons," Journal of Neurosurgery, vol. 128, no. 4, pp. 969–981, Apr. 2018, doi: 10.3171/2016.12.jns162262.

[9] A. Srinivasan, M. Goyal, F. A. Azri, and C. Lum, "State-of-the-Art Imaging of Acute Stroke," RadioGraphics, vol. 26, no. suppl_1, pp. S75–S95, Oct. 2006, doi: 10.1148/rg.26si065501.

[10] H. Masoumi, A. Behrad, M. A. Pourmina, and A. Roosta, "Automatic liver segmentation in MRI images using an iterative watershed algorithm and artificial neural network," Biomedical Signal Processing and Control, vol. 7, no. 5, pp. 429–437, Sep. 2012, doi: 10.1016/j.bspc.2012.01.002.

[11] J. C. Gore, "Artificial intelligence in medical imaging," *Magnetic Resonance Imaging*, vol. 68, pp. A1–A4, May 2020, doi: 10.1016/j.mri.2019.12.006.

[12] Hopyan et al., "Certainty of Stroke Diagnosis: Incremental Benefit with CT Perfusion over Noncontrast CT and CT Angiography," Radiology, vol. 255, no. 1, pp. 142–153, Apr. 2010, doi: 10.1148/radiol.09091021.

[13] M. Köhrmann and P. D. Schellinger, "Acute Stroke Triage to Intravenous Thrombolysis and Other Therapies with Advanced CT or MR Imaging: Pro MR Imaging," Radiology, vol. 251, no. 3, pp. 627–633, Jun. 2009, doi: 10.1148/radiol.2513081074.

[14] M. Wintermark, H. A. Rowley, and M. H. Lev, "Acute Stroke Triage to Intravenous Thrombolysis and Other Therapies with Advanced CT or MR Imaging: Pro CT," Radiology, vol. 251, no. 3, pp. 619–626, Jun. 2009, doi: 10.1148/radiol.2513081073.

[15] E. M. de Lucas et al., "CT Protocol for Acute Stroke: Tips and Tricks for General Radiologists," RadioGraphics, vol. 28, no. 6, pp. 1673–1687, Oct. 2008, doi: 10.1148/rg.286085502.

[16] K. Kawamoto, C. A. Houlihan, E. A. Balas, and D. F. Lobach, "Improving clinical practice using clinical decision support systems: a systematic review of trials to identify features critical to success," *BMJ*, vol. 330, no. 7494, p. 765, Mar. 2005, doi: 10.1136/bmj.38398.500764.8f.

[17] Y. Mokli, J. Pfaff, D. P. dos Santos, C. Herweh, and S. Nagel, "Computer-aided imaging analysis in acute ischemic stroke – background and clinical applications," Neurological Research and Practice, vol. 1, no. 1, Aug. 2019, doi: 10.1186/s42466-019-0028-y.

[18] W. Hacke et al., "Thrombolysis with Alteplase 3 to 4.5 Hours after Acute Ischemic Stroke," New England Journal of Medicine, vol. 359, no. 13, pp. 1317–1329, Sep. 2008, doi: 10.1056/nejmoa0804656.

[19] K. He, X. Zhang, S. Ren, and J. Sun, "Deep Residual Learning for Image Recognition," *2016 IEEE Conference on Computer Vision and Pattern Recognition (CVPR)*, Jun. 2016, doi: 10.1109/cvpr.2016.90.

[20] Z. Zhu, S. Lu, S.-H. Wang, J. M. Gorriz, and Y.-D. Zhang, "DSNN: A DenseNet-Based SNN for Explainable Brain Disease Classification," *Frontiers in Systems Neuroscience*, vol. 16, May 2022, doi: 10.3389/fnsys.2022.838822.

[21] A. Lisowska et al., "Context-Aware Convolutional Neural Networks for Stroke Sign Detection in Non-contrast CT Scans," Communications in Computer and Information Science, pp. 494–505, 2017, doi: 10.1007/978-3-319-60964-5_43.

[22] C.-M. Lo, P.-H. Hung, and D.-T. Lin, "Rapid Assessment of Acute Ischemic Stroke by Computed Tomography Using Deep Convolutional Neural Networks," *Journal of Digital Imaging*, May 2021, doi: 10.1007/s10278-021-00457-y.

[23] S. Mainali, M. Wahba, and L. Elijovich, "Detection of Early Ischemic Changes in Noncontrast CT Head Improved with 'Stroke Windows,'" ISRN Neuroscience, vol. 2014, pp. 1–4, Mar. 2014, doi: 10.1155/2014/654980.

[24] F. Macellari, M. Paciaroni, G. Agnelli, and V. Caso, "Neuroimaging in Intracerebral Hemorrhage," Stroke, vol. 45, no. 3, pp. 903–908, Mar. 2014, doi: 10.1161/strokeaha.113.003701.